

# Chlorination Chemistry. 1. Rate Coefficients, Reaction Mechanisms, and Spectra of the Chlorine and Bromine Adducts of Propargyl Halides

Dean B. Atkinson<sup>\*,†</sup> and Jeffrey W. Hudgens<sup>\*,‡</sup>

Physical and Chemical Properties Division, Chemical Science and Technology Laboratory,  
National Institute of Standards and Technology, Gaithersburg, Maryland 20899

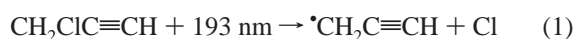
Received: March 29, 1999; In Final Form: August 6, 1999

Cavity ring-down spectroscopy (CRDS), end-product analysis, and ab initio calculations have determined absorption cross sections, rate coefficients, reaction mechanisms, and thermochemistry relevant to the addition of halogen atoms to propargyl chloride and propargyl bromide. Halogen atoms were produced by laser photolysis, and the addition reaction products were probed at a variable delay by CRDS using a second laser pulse. We report the continuum spectra of  $C_3H_3Cl_2$  (1,2-dichloroallyl),  $C_3H_3ClBr$  (1-chloro-2-bromoallyl), and  $C_3H_3Br_2$  (1,2-dibromoallyl) radicals between 238 and 252 nm and the absorption cross sections,  $\sigma_{240}(C_3H_3Cl_2) = (4.20 \pm 1.05) \times 10^{-17} \text{ cm}^2 \text{ molecule}^{-1}$  and  $\sigma_{242}(C_3H_3Br_2) = (1.04 \pm 0.31) \times 10^{-17} \text{ cm}^2 \text{ molecule}^{-1}$ . When the observed data are fit to complex reaction schemes, the 298 K rate coefficients for formation of 1,2-dihaloallyl radicals at 665 Pa were found to be  $k(Cl + C_3H_3Cl) = (1.2 \pm 0.2) \times 10^{-10} \text{ cm}^3 \text{ molecule}^{-1} \text{ s}^{-1}$  and  $k(Br + C_3H_3Br) = (2 \pm 1) \times 10^{-12} \text{ cm}^3 \text{ molecule}^{-1} \text{ s}^{-1}$ . At 298 K and 665 Pa the self-reaction rate coefficients of these radicals were found to be  $k(C_3H_3Cl_2 + C_3H_3Cl_2) = (3.4 \pm 0.9) \times 10^{-11} \text{ cm}^3 \text{ molecule}^{-1} \text{ s}^{-1}$  and  $k(C_3H_3Br_2 + C_3H_3Br_2) = (1.7 \pm 1.1) \times 10^{-11} \text{ cm}^3 \text{ molecule}^{-1} \text{ s}^{-1}$ . The listed uncertainties are twice the standard deviation of individual determinations, and those for rate coefficients include the uncertainty of the appropriate absorption cross section.

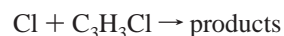
## Introduction

When attempting to formulate numeric models that describe the manufacture or destruction (e.g., combustion, pyrolysis, or plasma processes) of industrially important halogenated chemicals, one finds that few of the relevant reaction rate coefficients and reaction mechanisms are known. For example, only a few rate coefficients for halogen addition to unsaturated hydrocarbons are available. This lack of information may arise because of the practical problems of such studies. Addition to a multiple bond necessarily involves at least two carbons, which can lead to distinct isomers. Since isomers commonly possess similar optical and mass spectra, dynamic measurements of species concentrations become very difficult. As a result, neither the spectra nor the reaction rate coefficients pertaining to most halogen adducts are known. Furthermore, this dearth of experimental data may account for the absence of computational results capable of supporting such experimental measurements.

Our interest in the reactions of halogen atoms with propargyl halides ( $CH_2XC\equiv CH$ , where  $X = Cl, Br$ ) originated with measurements of the self-reaction rate coefficient for the propargyl radical ( $\cdot CH_2C\equiv CH$ ). Our measurements,<sup>1</sup> like those by others,<sup>2–4</sup> were initiated by photolyzing propargyl halides. The photolysis of propargyl chloride (3-chloropropyne) with 193 nm light is particularly clean, since 93% of the photolysis yield is propargyl radicals:<sup>2</sup>



This photolytic process also generates an equal concentration of chlorine atoms. Since chlorine atoms may react with the propargyl chloride parent,  $C_3H_3Cl$ , to produce secondary radical products that cross-react with propargyl radicals ( $C_3H_3$ ), we needed to account for this companion chemistry to ensure that our derived  $k(C_3H_3 + C_3H_3)$  rate coefficient was not contaminated by unaccounted side reactions. When we began to investigate the chemistry initiated by the chlorine atoms, we found that the fundamental nature of the simple reaction



is rife with uncertainty. On one hand, a recent study reported that chlorine atoms react with  $C_3H_3Cl$  to generate  $Cl_2$  and more propargyl radicals, effectively doubling the  $C_3H_3$  yield of reaction 1.<sup>5</sup> On the other hand, previous studies of chlorine reactions with olefins and with acetylene would support the hypothesis that chlorine atoms add onto  $C_3H_3Cl$  at the triple bond, forming unsaturated radicals.<sup>6–10</sup> If chlorine adds to  $C_3H_3Cl$ , more questions arise: Does addition occur at the center or terminal unsaturated carbon atoms? Do adduct radicals possess vinylic structures, or have they isomerized into the more stable allylic structures? Since each vinylic and allylic structure possesses more than one isomer, which ones are dominant? Finally, we wished to assess the impact of these products upon determinations of  $k(C_3H_3 + C_3H_3)$ .

In this account we report experiments and calculations that explicate the mechanism governing the addition reactions of chlorine and bromine atoms with propargyl halides. Using a recently developed apparatus that uses laser photolysis and

<sup>†</sup> NIST/NRC Postdoctoral Associate 1995–1997. Current address: Chemistry Department, Portland State University, Portland, OR 97207-0751. E-mail: atkinsond@pdx.edu.

<sup>‡</sup> E-mail: jeffrey.hudgens@nist.gov.

cavity ring-down detection,<sup>11</sup> we have observed ultraviolet absorption spectra of the radical adducts  $C_3H_3Cl_2$ ,  $C_3H_3ClBr$ , and  $C_3H_3Br_2$ . Within this apparatus we have also measured the rate coefficients of chlorine atom addition to propargyl chloride and of bromine atom addition to propargyl bromide (3-bromopropyne). The self-reaction rate coefficients for  $C_3H_3Cl_2$  and  $C_3H_3Br_2$  radicals at 298 K were also determined. The combination of analyses of the stable photolysis products and ab initio computational results have enabled us to determine and assign the reactive species.

### Experimental Procedure<sup>12</sup>

The details of the laser photolysis and cavity ring-down (CRD) apparatus are described elsewhere,<sup>11</sup> so this section presents only a basic overview and recent experimental refinements. A 16 mm i.d. quartz tube forms the reactor through which a premixed gas of known composition flows. The pumping rate is adjusted so that the movement of the gas sample along the flow axis is inconsequential within the time interval of a single kinetic measurement, yet fast enough that the reaction mixture is fully refreshed during the 200 ms between laser pulses.<sup>1</sup>

Initially, an excimer laser (ArF producing 193 nm, nominal 20 ns pulse, maximum pulse energy of 100 mJ or XeF producing 351 nm, nominal 20 ns pulse, maximum pulse energy of 200 mJ) photolyzes the reaction mixture. The photolysis laser beam is expanded and masked to produce a uniform block 67 mm wide and 20 mm high with a peak power density of less than 100 kW cm<sup>-2</sup>. Subsequently, the absorption by a selected species is measured with cavity ring-down absorption spectroscopy. For the CRDS we used a 1.1 m long cavity formed by two concave mirrors (1.0 m radius of curvature;  $R^* > 99.6\%$  @ 245 nm; VLOC, Inc.) of high effective reflectivity<sup>11</sup> and a usable bandwidth of about  $\pm 7$  nm ( $R^* > 98\%$ ). At 245 nm the cavity exhibited an exponential decay with a base 1/e ring-down time of 1.3  $\mu$ s. The ring-down cavity lies along the flow axis, normal to the photolysis beam direction, so that the width of the photolysis beam defines the path length of the transient absorbing species. This optical configuration makes the extraction of species density straightforward. To minimize effects from radial gradients of photolysis products, the photolysis beam height is larger than the diameter of the reactor tube and the probe beam diameter inside the cavity (beam waist of  $TEM_{max} \approx 0.32$  mm) is much smaller than the flow tube inner dimension.

The tunable probe laser beam was produced by an excimer-pumped dye laser (nominal 20 ns pulse width; laser dye, coumarin 480; BBO doubling crystal). At the cavity entrance mirror an iris apertured the probe laser beam to  $\sim 2$  mm diameter and the energy was not allowed to exceed 100  $\mu$ J/cm<sup>2</sup>/pulse. The photomultiplier signal was (analog) filtered to pass frequencies less than 25 MHz. (Proper cavity alignment was verified by observing oscilloscope traces recorded at the full 1.0 GHz bandwidth.) A fit to each exponential ring-down trace was extracted from a weighted linear regression of a semilog plot and yielded the decay rate. We verified the quality of this procedure by fitting the data using an iterative, nonlinear Levenberg–Marquardt fitting routine.<sup>13</sup> Both methods yielded the same values. We note that CRD absorbance measurements have been demonstrated to obey the Beer–Lambert relationship for the broad transitions often encountered in the ultraviolet spectrum.<sup>11</sup>

Cavity ring-down measurements indicate an enhanced rate of decay of photon intensity in a stable optical cavity. The difference between this rate and the decay rate under nonabsorbing conditions (base decay rate) is proportional to the

absorbance of the transient species. In this experiment the base decay rate is periodically measured by probing the reaction mixture at a time prior to the photolysis laser pulse. This procedure also allows us to compensate for diminished cavity performance during the experiment. In principle, this procedure for determining absorbance may suffer a small offset error due to the effects of thermal lensing within the cavity; however, we did not observe any offset. Proper baselines were obtained over the spectral intervals indicating that the photofragments carried no absorbance. The decay or growth of the monitored species absorption is observed by changing the delay time between the photolysis and probe (CRD) laser pulses. To minimize the effects of long-term drift in the photolysis efficiency, the time interval between the photolysis and probe pulses is randomly selected between zero and preset values. During experiments that used 193 nm light to photolyze propargyl halides, random time sampling was particularly important because the reaction tube would gradually accumulate brown soot in the photolysis region. When required, this soot was easily washed from the apparatus with soap and water. Presumably, the soot arises from reactions involving propargyl radicals.<sup>14</sup> Experiments that used 351 nm light did not produce propargyl radicals and soot.

Chlorine (99.9% stated purity, 10% Cl<sub>2</sub> in helium) was used as supplied.  $C_3H_3Cl$  (Aldrich, 98% stated purity) and  $C_3H_3Br$  (Fluka, 98% stated purity) were freeze–thaw degassed in liquid nitrogen to remove any volatile contaminants, and then 5%–10% mixtures in the buffer gas were prepared and stored in blackened glass bulbs. All reactant and buffer gases were flowed through mass flow controllers (MKS model 1259C).

The kinetics experiments produce transient absorption (which is readily converted to radical concentration) vs time. To derive rate coefficients from these data, a kinetic mechanism is presumed and the absorption data are numerically simulated on a computer. This simulation is compared to the observed data, and the  $\chi^2$  value is computed. By use of the Levenberg–Marquardt procedure, selected rate coefficients and concentrations are varied to minimize this value. The simulation software is comprised of a customized graphic interface that spawns satellite shells executing the original FORTRAN code of the ACUCHEM kinetics simulation program.<sup>15</sup> ACUCHEM contains a symbolic interpreter, allowing the input of the kinetic model in an intuitive format, and a numerical forward integration routine, the accuracy of which has been described and verified previously.<sup>15</sup>

GC–MS end-product analyses of irradiated samples were accomplished with a HP 5890 series 2 gas chromatograph (GC) that is coupled to an HP 5972 mass spectrometer. The GC was equipped with a Restek model 502.2 column (0.32 mm i.d.  $\times$  30 m long). The irradiated samples were injected into a gas chromatograph, and the mass spectra of the eluted peaks were recorded.

Ab initio calculations were performed with the Gaussian 94 program suite.<sup>16</sup>

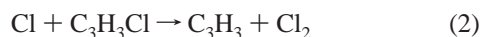
### Results and Analyses

**Absorption Spectra and Identification of the Spectral Carriers.** This study began as a spectroscopic search for strong absorption bands of propargyl radicals that could support measurements of propargyl radical rate coefficients. We produced propargyl radicals by photolyzing propargyl halides. Propargyl halides exposed to 193 nm light decompose along two channels:



Morter et al.<sup>2</sup> have measured the photolysis branching ratio of propargyl chloride and found that reaction 1a accounts for 93% of the products. Slagle et al.<sup>3</sup> used mass spectrometry to measure HBr yields and found that reaction 1a accounts for 50%, or less, of the propargyl bromide photoproducts.

A recent study reported the discovery of a new absorption band of propargyl radical between 230 and 270 nm among the 193 nm photolysis products of propargyl chloride.<sup>5</sup> The spectrum displayed an absorption maximum at  $\lambda_{\text{max}} = 242$  nm, and the intensity declined to  $0.25I(\lambda_{\text{max}})$  at 252 nm. Following the 193 nm laser photolysis event, the signal was observed to increase on two time scales. The “instant” signal was attributed to reaction 1a. The slower growth of absorbance to twice the prompt signal was attributed to the reaction

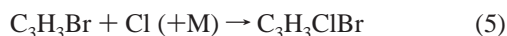
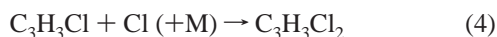


in which chlorine atoms are produced from reaction 1a. This temporal behavior led to the conclusion that the spectra arose from the propargyl radical.<sup>5</sup>

When we photolyzed propargyl chloride, we observed the same spectrum that was reported in ref 5. Figure 1a shows the CRD spectrum of the 193 nm photolysis products from propargyl chloride. As in ref 5, the CRD spectrum exhibits an absorption maximum at  $\lambda_{\text{max}} = 240$  nm and the absorption intensity degrades to  $0.25I(\lambda_{\text{max}})$  at 252 nm. In contrast, the temporal traces of the absorption at 242 nm exhibited only a rapid, continuous growth to maximum signal. No prominent instant absorption signal was observed. Despite this difference of temporal behavior, we believe that the carrier of this and the carrier of the spectrum in the previous study are identical.

We attempted to verify that the spectrum originated from propargyl radicals by observing the absorption by the photolysis products of propyne and allene. When exposed to 193 nm light, both unhalogenated precursors are known to produce propargyl radicals;<sup>1,17,18</sup> although for propyne, propargyl radicals may be formed through the rapid secondary reaction between the nascent  $\text{CH}_3\text{C}\equiv\text{C}\cdot$  products<sup>19–21</sup> and the propyne background bath.<sup>1</sup> Since neither precursor reproduced the transient absorption spectrum between 238 and 252 nm, we concluded that the propargyl radical does not account for the spectrum of Figure 1a. We also concluded that the transient radical contains at least one chlorine atom.

Experiments that used 351 nm photolysis to initiate reactions were used to confirm the activity of the chlorine atom addition reaction. Mixtures of helium, propargyl chloride, and propargyl bromide produced no transient spectra, showing that they are inert to 351 nm light. When exposed to 351 nm light,  $\text{Cl}_2$  dissociates.<sup>9</sup> When  $\text{Cl}_2$  was added to the reactor flow, 351 nm light induced transient absorption signals between 238 and 252 nm. This result is consistent with the reaction sequence



Curves b and c of Figure 1 show the absorption spectra observed from the products of each reaction. The spectrum of  $\text{Cl} + \text{C}_3\text{H}_3\text{Cl}$  (Figure 1b) is identical to the spectrum of  $\text{C}_3\text{H}_3\text{-Cl}$  photolyzed by 193 nm light (Figure 1a), indicating that both

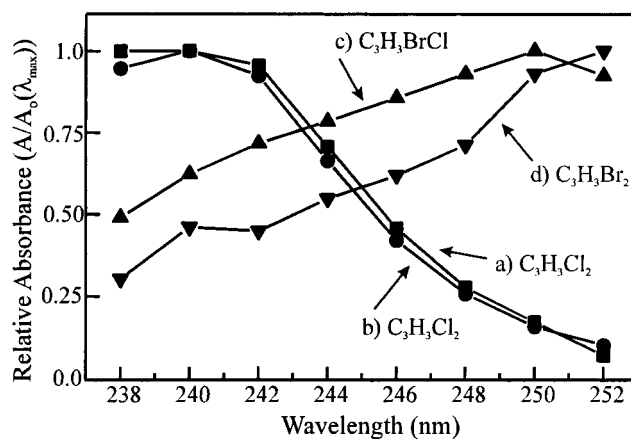
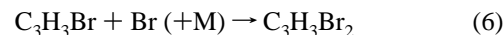


**Figure 1.** Ultraviolet absorption spectra between 238 and 252 nm observed from (a)  $\text{C}_3\text{H}_3\text{Cl}_2$  (1,2-dichloroallyl) radicals formed by 193 nm photolysis of propargyl chloride, (b)  $\text{C}_3\text{H}_3\text{Cl}_2$  radicals formed by  $\text{Cl} + \text{propargyl chloride}$ , (c)  $\text{C}_3\text{H}_3\text{BrCl}$  (1-chloro-2-bromoallyl) radicals formed by  $\text{Cl} + \text{propargyl bromide}$ , and (d)  $\text{C}_3\text{H}_3\text{Br}_2$  (tentatively assigned as 1,2-dibromoallyl) radicals formed by  $\text{Br} + \text{propargyl bromide}$ . Each plot is normalized to the absorption maximum of the species.

spectra arise from the same adduct. The spectrum produced by reaction 5 differs from that from reaction 4, indicating that its spectral carrier contains at least one bromine and at least one chlorine atom.

Previous studies<sup>1,2,17,18</sup> have shown that 193 nm photolysis of propargyl bromide generates propargyl radicals and Br atoms. Morter et al.<sup>2</sup> found that nascent Br atoms decayed rapidly and suggested that they were reacting with propargyl bromide:



When propargyl bromide was photolyzed at 193 nm, we observed a transient absorption spectrum with  $\lambda_{\text{max}} \approx 252$  nm (Figure 1d). Although featureless, the product of reaction 6 displays a spectrum that is red-shifted relative to photolyzed  $\text{C}_3\text{H}_3\text{Cl}$ . The red-shifted transient spectra obtained from reactions 5 and 6 are consistent with the observation that the electronic origins of analogous halogenated radicals display red shifts as bromine is substituted for chlorine.<sup>22,23</sup> The spectrum obtained from reaction 6 is also distinct from that of reaction 5. As expected for a set of distinct spectral carriers, each spectrum produced by reactions 4–6 has a characteristic rise time (between 20 and 1000  $\mu\text{s}$ ) and fall time (between 10 and 20 ms).

Figure 2 shows a time-resolved trace of the transient absorption at 242 nm observed from the products of propargyl bromide (reaction 6). Immediately after the 193 nm photolysis event, the photolysis products of propargyl bromide showed a prompt increase in absorbance, which is noted in Figure 2 with the arrow labeled  $t_0$ . One or both, of the nascent products,  $\text{C}_3\text{H}_3$  and  $\text{C}_3\text{H}_2$ , are the candidate carriers of this absorption. However, the same photolysis experiments using propargyl chloride did not exhibit strong prompt absorption. Since propargyl chloride has a large quantum yield of  $\text{C}_3\text{H}_3$  radicals ( $\Phi_{\text{C}_3\text{H}_3} = 93\%$ ),<sup>2</sup> the absence of a strong prompt absorption allows us to discard  $\text{C}_3\text{H}_3$  from consideration and to assign the absorption to one of the  $\text{C}_3\text{H}_2$  carbenes. Vinylidenecarbene ( $\text{CH}_2\text{C}=\text{C}\cdot$ ) appears as the most likely carrier of this signal because it absorbs strongly between 240 and 250 nm.<sup>24,25</sup> Assignments to the propynylidene or cyclopropenylidene structures are not supported because their absorption bands reside outside the spectral interval.<sup>24</sup>



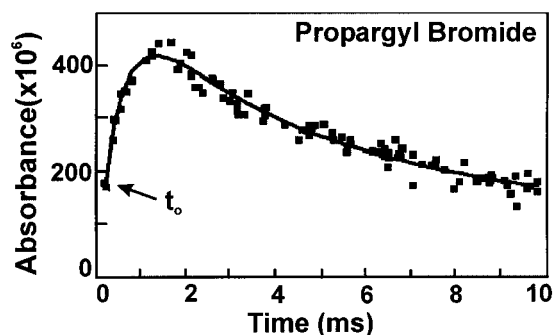


**Figure 2.** Plots of the composite transient absorbance at 242 nm observed when propargyl bromide was photolyzed with 193 nm light at 298 K. The increase of the  $C_3H_3Br_2$  radical signal is dominated by the reaction  $Br + C_3H_3Br$ , and the signal decay is dominated by  $C_3H_3Br_2 + C_3H_3Br_2$ . The solid line shows the best fit of the signal decay derived using the model given in Table 3. The arrow, labeled  $t_0$ , denotes the prompt absorption by nascent  $C_3H_2$ .

**GC-MS Analysis of the End Products.** To determine the products of reaction 4, we conducted end-product analysis experiments. A bulb equipped with fused quartz windows was filled with a 1%  $C_3H_3Cl/99\%$  He molar mixture to 101 kPa (1 atm) and irradiated with 193 nm laser light at 1 Hz. We found that exposure to 100 laser pulses at 30 mJ/pulse was the minimum irradiation required to produce measurable products. The volatile products of the irradiated samples were separated on a gas chromatograph, and the eluents were analyzed with a mass spectrometer. The eluents included two  $C_6H_6$  species (1,5-hexadiyne was confirmed, and 1,2-hexadien-5-yne was tentatively assigned) that are produced by recombination of propargyl radicals. We present the reaction mechanisms governing their production elsewhere.<sup>1</sup>

The gas chromatograph eluted three chlorinated photolysis products. The first chlorinated  $C_3$  product that eluted from the GC column exhibits a mass spectrum consistent with its assignment as chloroallene.<sup>26</sup> We confirmed the identity of the other two  $C_3H_4Cl_2$  species by matching their retention times and mass spectra with those of pure reagent samples. The dominant  $C_3H_4Cl_2$  species of >95% abundance (referenced to total  $C_3H_4Cl_2$  yield) was 2,3-dichloro-1-propene and an almost undetectable second species of abundance <5% was (*Z*)-1,3-dichloro-1-propene. (*E*)-1,3-Dichloro-1-propene, which is the lesser fraction in commercial samples of 1,3-dichloro-1-propene, was not detected. When the relative detection efficiencies of products were ignored, the abundance ratio of the chloroallene to 2,3-dichloro-1-propene products was 3:1.

The dominance of the 2,3-dichloro-1-propene over 1,3-dichloro-1-propene among the end products indicates that the persistent free radicals formed by reaction 4 contain two chlorine atoms bound to adjacent carbon atoms. The candidates are the 2,3-dichloro-1-propene-1-yl radical ( $CH_2ClCCl=CH^*$ ), the 1,2-dichloroallyl radical ( $CH_2\dot{C}Cl-CHCl$ ), and a mixture composed of both radicals. In subsequent sections we will present the results of ab initio calculations and interpret the end-product data as evidence that the 1,2-dichloroallyl radical is the only persistent free radical formed by reaction 4. We will also show that the newly added chlorine is located on the end carbon of the 1,2-dichloroallyl radical. By analogy, we expect other products of chlorine and bromine atom addition to propargyl halides to contain the newly added halogen on the end carbon. In the Discussion, we will complete the rationale for assigning the products of reactions 4, 5, and 6 to the 1,2-dichloroallyl radical, the 1-chloro-2-bromoallyl radical, and the 1,2-dibromoallyl radical, respectively.

**Optical Absorption Cross-Section Measurements.** The absorption cross sections of the  $C_3H_3Cl_2$  and  $C_3H_3Br_2$  radicals were determined at 240 nm using chemical actinometry. Within the bandwidth of our laser ( $\Delta\nu \approx 0.3 \text{ cm}^{-1}$ ), the spectra exhibit no evidence of fine structure. The absence of structure indicates that these bands are absorption continua and are ideal for absorption measurements with cavity ring-down spectroscopy. The extinction coefficient remains essentially constant across the bandwidth of the laser beam, causing each populated cavity mode to decay at the same rate.<sup>27</sup> The uniformity of these optical decay rates enables accurate concentration measurements.

We measured the absolute absorption cross section of the  $C_3H_3Cl_2$  radical at 240 nm by comparing it with the absorption cross section of the  $C_3H_4Cl$  radical. This method uses the simple reaction mechanisms initiated by the photolysis of  $Cl_2$  with 351 nm light. A mixture of helium, chlorine, and excess propargyl chloride was flowed through the reactor. The 351 nm laser photolysis pulse produced chlorine atoms (reaction 3) that quantitatively generate 1,2-dichloroallyl radicals via reaction 4. The transient absorption maximum at 240 nm was measured. Immediately following this measurement, we replaced the propargyl chloride flow with allene. The photolysis pulse from a XeF laser produced Cl atoms (reaction 3) that rapidly reacted with allene:



The transient absorbance of this mixture was measured. Since the chlorine flow rate and excimer laser energy remained constant throughout these experiments, the absorption measurements assayed equal amounts of  $C_3H_3Cl_2$  and  $C_3H_4Cl$  radicals. The ratio of absorbances,  $A_{240}^{C_3H_3Cl_2}/A_{240}^{C_3H_4Cl} = 1.64$ , was multiplied by our absorption cross section of the  $C_3H_4Cl$  radical at 240 nm,  $\sigma_{240}(C_3H_4Cl) = (2.5 \pm 0.5) \times 10^{-17} \text{ cm}^2 \text{ molecule}^{-1}$ <sup>28</sup> to yield  $\sigma_{240}(C_3H_3Cl_2) = (4.2 \pm 1.05) \times 10^{-17} \text{ cm}^2 \text{ molecule}^{-1}$ . The uncertainties of this and all absorption coefficients derived in this report are specified for two standard deviations (i.e., type A uncertainty with a coverage factor of 2 (see ref 29)).

The absolute absorption cross sections of the  $C_3H_2$  carbene and  $C_3H_3Br_2$  radical at 242 nm were estimated by comparing them with the absorption cross section of the propargyl ( $C_3H_3$ ) radical. Promptly after the photolysis pulse, the nascent photoproducts are at their maximum concentrations. The prompt absorption at 242 nm arises only from  $C_3H_2$ . The prompt absorption at 332.5 nm arises only from propargyl radicals. Experiments measured these prompt absorptions under the same conditions and indicate the ratio,  $A_{242}^{C_3H_2}(t=0)/A_{332.5}^{C_3H_3}(t=0) = 0.5$ . This ratio yields the absorption cross section of  $C_3H_2$  using

$$\sigma_{242}(C_3H_2) = \frac{\Phi_{C_3H_3} \left[ A_{242}^{C_3H_2}(t=0) \right]}{\Phi_{C_3H_3} \left[ A_{332.5}^{C_3H_3}(t=0) \right]} \sigma_{332.5}(C_3H_3) \quad (8)$$

where  $\Phi_k$  is the quantum yield of the indicated species and  $\sigma_{332.5}(C_3H_3) = (4.13 \pm 0.6) \times 10^{-18} \text{ molecule}^{-1} \text{ cm}^2$ .<sup>1</sup> To compute this cross section, we have assumed the upper limit of the branching ratio of reaction 1a to be  $f_{1a} = \Phi_{C_3H_3} = 0.5$ , estimated previously from mass spectrometry data.<sup>3</sup> Adoption of  $\Phi_{C_3H_3} = \Phi_{C_3H_2} = 0.5$  yields the value  $\sigma_{242}(C_3H_2) = (2.06 \pm 0.6) \times 10^{-18} \text{ cm}^2 \text{ molecule}^{-1}$ .

The absorption cross section of the  $C_3H_3Br_2$  radical is computed from the transient absorption maximum at 242 nm that is observed nearly 1 ms after the photolysis event. The maximum transient absorption at 242 nm and the prompt absorption at 332.5 nm (by  $C_3H_3$ ) gave the ratio  $A_{242}^{\text{Max}}(t)/$

**TABLE 1: Kinetic Model and Derived Rate Coefficients That Interpret the Signal Traces Produced by 351 nm Photolysis of Mixtures Containing Cl<sub>2</sub>/C<sub>3</sub>H<sub>3</sub>Cl in N<sub>2</sub> Buffer at 298 K<sup>a</sup>**

reaction	rate coefficient, <sup>b</sup> cm <sup>3</sup> molecule <sup>-1</sup> s <sup>-1</sup>	comments
Cl <sub>2</sub> + 351 nm → 2Cl		
C <sub>3</sub> H <sub>3</sub> Cl + Cl (+ M) → C <sub>3</sub> H <sub>3</sub> Cl <sub>2</sub>	(1.2 ± 0.2) × 10 <sup>-10</sup>	fitted rate of this study
C <sub>3</sub> H <sub>3</sub> Cl <sub>2</sub> + C <sub>3</sub> H <sub>3</sub> Cl <sub>2</sub> (+M) → product	(3.4 ± 0.9) × 10 <sup>-11</sup>	fitted rate of this study

<sup>a</sup> The experiments monitored the C<sub>3</sub>H<sub>3</sub>Cl<sub>2</sub> (1,2-dichloroallyl) radical concentration at 242 nm. <sup>b</sup> Uncertainties denote two standard deviations including the propagated uncertainty of the absorption cross section.

$A_{332.5}^{C_3H_3}(t=0) = 1.50$ . The cross section was computed using

$$\sigma_{242}(C_3H_3Br_2) = \frac{1}{f_{Br}(t)} \left( \frac{A_{242}^{Max}(t)}{A_{332.5}^{C_3H_3}(t=0)} \right) - \frac{f_{C_3H_2}(t)}{f_{Br}(t)} \left( \frac{A_{242}^{C_3H_2}(t=0)}{A_{332.5}^{C_3H_3}(t=0)} \right) \sigma_{332.5}(C_3H_3) \quad (9)$$

where  $f_{C_3H_2}(t)$  describes the fractional loss of C<sub>3</sub>H<sub>2</sub> vs time. The term  $f_{Br}(t)$  describes the fractional conversion of nascent Br atoms into C<sub>3</sub>H<sub>3</sub>Br<sub>2</sub> and the subsequent loss of C<sub>3</sub>H<sub>3</sub>Br<sub>2</sub> vs time. Since the absorption maximum at 242 nm occurs at  $t \approx 1$  ms after the photolysis event, secondary reactions diminish  $f_{C_3H_2}(t)$  and  $f_{Br}(t)$  from unity. Recursive computations of the chemical model and equation 9 converged to give  $\sigma_{242}(C_3H_3Br_2) = (1.5 \pm 0.4) \times 10^{-17}$  cm<sup>2</sup> molecule<sup>-1</sup>. At the absorption maximum the chemical model (shown in the following) found that  $f_{C_3H_2}(t) \approx 0.01$  and  $f_{Br}(t) \approx 0.4$ . The accuracy of this cross section is largely limited by the accuracy of the presumed branching ratio for reaction 1.

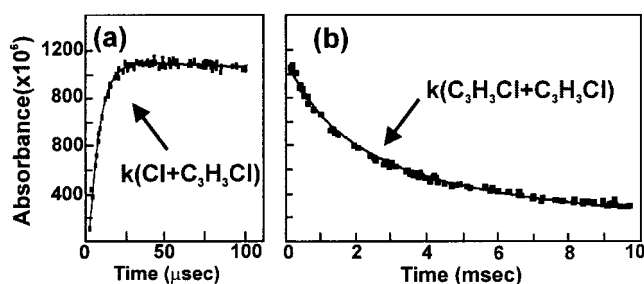
#### Rate Coefficients in the Cl<sub>2</sub>/Propargyl Chloride System.

Table 1 summarizes the kinetic reaction scheme used to fit the rise and decay of C<sub>3</sub>H<sub>3</sub>Cl<sub>2</sub> formed by the 351 nm photolysis of mixtures containing Cl<sub>2</sub>, propargyl chloride, and N<sub>2</sub> buffer. During these experiments the Cl<sub>2</sub> partial pressure was fixed at 52 Pa, the propargyl chloride partial pressure was varied between 5.2 and 52 Pa, and the N<sub>2</sub> buffer was adjusted to maintain a total pressure of 625 Pa (4.7 Torr).

The kinetic model (Table 1) necessary to fit the experimental data is comprised of only three reactions. In the presence of the large excess of C<sub>3</sub>H<sub>3</sub>Cl in the reaction mixture, side reactions involving Cl atoms are strongly suppressed by their rapid addition rate to C<sub>3</sub>H<sub>3</sub>Cl. Although we cannot rule out a side reaction between C<sub>3</sub>H<sub>3</sub>Cl<sub>2</sub> and Cl<sub>2</sub>, such a side reaction would generate a chlorine atom that would react with C<sub>3</sub>H<sub>3</sub>Cl (reaction 4), conserving the concentration of C<sub>3</sub>H<sub>3</sub>Cl<sub>2</sub>. This secondary reaction process would not affect the analysis of these experiments.

In this work the kinetic models used to analyze data do not contain contributions from wall reactions. Wall reactions are minimized largely because the beam waist of the CRD cavity is small compared to the reactor diameter. This simplification is also justified by the results of a numerical model of radial diffusion between the CRD axis and the reactor walls. This diffusion model predicts that wall losses may begin to affect the CRD signal for times exceeding 20 ms. Thus, we use data observed prior to this time for derivations of reaction rate coefficients.

The concentration of C<sub>3</sub>H<sub>3</sub>Cl<sub>2</sub> was monitored by CRDS at 242 nm. Figure 3a shows the data obtained by a typical experiment and the fit that extracts one determination of the addition rate coefficient. The fits of signal traces of 50 and 100 μs duration (100 randomly spaced measurement points) after the photolysis gave an average addition rate coefficient at 298



**Figure 3.** Plots of the transient absorbance at 240 nm observed when a mixture of Cl<sub>2</sub> and propargyl chloride was photolyzed with 351 nm light at 298 K. (a) Increase of the C<sub>3</sub>H<sub>3</sub>Cl<sub>2</sub> (1,2-dichloroallyl) radical signal produced by the reaction Cl + C<sub>3</sub>H<sub>3</sub>Cl. The solid line shows the fit that gives one determination of the pseudo-first-order rate coefficient  $k(\text{Cl} + \text{C}_3\text{H}_3\text{Cl})$ . (b) Pure second-order decay of C<sub>3</sub>H<sub>3</sub>Cl<sub>2</sub> radical due to the self-reaction C<sub>3</sub>H<sub>3</sub>Cl<sub>2</sub> + C<sub>3</sub>H<sub>3</sub>Cl<sub>2</sub>. The solid line shows the fit of these data, which provides one determination of the second-order rate coefficient  $k(\text{C}_3\text{H}_3\text{Cl}_2 + \text{C}_3\text{H}_3\text{Cl}_2)$ . Both traces are plotted on the same absorbance scale.

K,  $k(\text{Cl} + \text{C}_3\text{H}_3\text{Cl}) = (1.2 \pm 0.2) \times 10^{-10}$  cm<sup>3</sup> molecule<sup>-1</sup> s<sup>-1</sup>, where in this paper all rate coefficients are specified with the uncertainty of two standard deviations (i.e., the type A uncertainty with a coverage factor of 2 (see ref 29)). According to the fits, the typical photolysis event dissociated about 0.46% of the irradiated Cl<sub>2</sub>. While keeping  $k(\text{Cl} + \text{C}_3\text{H}_3\text{Cl})$  fixed to the previously determined average, we derived the self-reaction rate coefficient at 298 K,  $k(\text{C}_3\text{H}_3\text{Cl}_2 + \text{C}_3\text{H}_3\text{Cl}_2) = (3.4 \pm 0.9) \times 10^{-11}$  cm<sup>3</sup> molecule<sup>-1</sup> s<sup>-1</sup>, by fitting signal traces of 4 and 10 ms duration. This uncertainty denotes two standard deviations and propagates the uncertainty of  $\sigma_{242}(C_3H_3Cl_2)$ . Figure 3b shows typical data and the fit that extracts a measurement of the self-reaction rate coefficient. The nearly pure second-order decay of the absorption signal indicates that C<sub>3</sub>H<sub>3</sub>Cl<sub>2</sub> does not react (or reacts very slowly) with propargyl chloride.

#### Cross-Reaction Rate Coefficient for C<sub>3</sub>H<sub>3</sub> + C<sub>3</sub>H<sub>3</sub>Cl<sub>2</sub>.

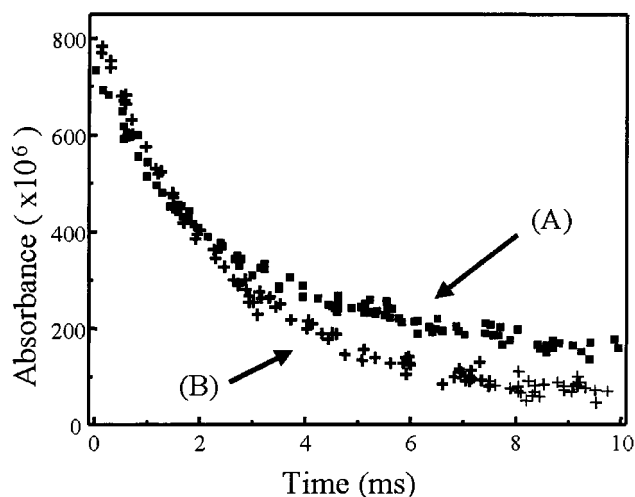
Table 2 summarizes the mechanism used to fit the rise and decay of C<sub>3</sub>H<sub>3</sub>Cl<sub>2</sub> formed by the 193 nm photolysis of mixtures containing propargyl chloride and helium buffer. These experiments were conducted with the propargyl chloride partial pressure set between  $6 \times 10^{-4}$  Pa and 0.22 Pa. The helium buffer was varied to produce a range of total pressures between 505 and 1270 Pa (3.8 and 9.5 Torr). The concentration of C<sub>3</sub>H<sub>3</sub>Cl<sub>2</sub> was monitored by CRDS at 242 nm. According to the fit, the photolysis event dissociated between 0.2% and 0.6% of the irradiated propargyl chloride. The photolysis yield variation reflects the range of 193 nm pulse energies and the changing attenuation of the photolysis beam by soot, noted earlier. During each individual kinetic determination the average pulse energy transmitted through the photolysis zone declined by less than 1%. The rate of this diminishing photolysis energy is too gradual to effect the derived rate coefficients.

Table 2 shows the kinetic model used to fit the absorption decay observed at 242 nm that was initiated by the photolysis of propargyl chloride with 193 nm light. Following the photolysis event, the chlorine atoms react quantitatively with

**TABLE 2: Kinetic Model and Derived Rate Coefficients Used to Interpret the Signal Traces Produced by 193 nm Photolysis of C<sub>3</sub>H<sub>3</sub>Cl in Helium Buffer at 298 K<sup>a</sup>**

reaction	rate coefficient, <sup>b</sup> cm <sup>3</sup> molecule <sup>-1</sup> s <sup>-1</sup>	comments
C <sub>3</sub> H <sub>3</sub> Cl + 193 nm → C <sub>3</sub> H <sub>3</sub> + Cl	$f_{1a} = 0.93$	branching ratio adopted from ref 2
C <sub>3</sub> H <sub>3</sub> Cl + 193 nm → C <sub>3</sub> H <sub>2</sub> + HCl	$f_{1b} = 0.07$	branching ratio adopted from ref 2
C <sub>3</sub> H <sub>3</sub> Cl + Cl (+M) → C <sub>3</sub> H <sub>3</sub> Cl <sub>2</sub>	$1.2 \times 10^{-10}$	unadjusted rate adopted from Table 1
C <sub>3</sub> H <sub>3</sub> Cl <sub>2</sub> + C <sub>3</sub> H <sub>3</sub> Cl <sub>2</sub> (+M) → products	$3.4 \times 10^{-11}$	unadjusted rate adopted from Table 1
C <sub>3</sub> H <sub>3</sub> + C <sub>3</sub> H <sub>3</sub> (+M) → C <sub>6</sub> H <sub>6</sub>	$4.3 \times 10^{-11}$	unadjusted rate from ref 1
C <sub>3</sub> H <sub>3</sub> + C <sub>3</sub> H <sub>3</sub> Cl <sub>2</sub> → products	$(7 \pm 6) \times 10^{-11}$	fitted rate of this study
Cl + C <sub>3</sub> H <sub>3</sub> Cl <sub>2</sub> (+M) → C <sub>3</sub> H <sub>3</sub> Cl <sub>3</sub>	$1.5 \times 10^{-10}$	unadjusted value adopted for preliminary fits and deleted from final fit (see text)
C <sub>3</sub> H <sub>3</sub> + Cl (+M) → C <sub>3</sub> H <sub>3</sub> Cl	$1.5 \times 10^{-10}$	unadjusted value adopted for preliminary fits and deleted from final fit (see text)

<sup>a</sup> The experiments monitored the C<sub>3</sub>H<sub>3</sub>Cl<sub>2</sub> (1,2-dichloroallyl) radical concentration at 242 nm. <sup>b</sup> Uncertainties denote two standard deviations including the propagated uncertainty of the absorption cross section.



**Figure 4.** Time-resolved plot of absorbance by C<sub>3</sub>H<sub>3</sub>Cl<sub>2</sub> (1,2-dichloroallyl radical) at 242 nm following (a) the photolysis of a mixture of Cl<sub>2</sub> and propargyl chloride with 351 nm light (trace A; solid squares) and (b) the photolysis of propargyl chloride with 193 nm light (crosses). Both reactions were run in helium buffer at approximately 660 Pa (5 Torr) total pressure. The decay of trace A reflects the rate coefficient  $k(\text{C}_3\text{H}_3\text{Cl}_2 + \text{C}_3\text{H}_3\text{Cl}_2)$ . The decay of trace B reflects the rate coefficients  $k(\text{C}_3\text{H}_3\text{Cl}_2 + \text{C}_3\text{H}_3\text{Cl}_2)$  and  $k(\text{C}_3\text{H}_3 + \text{C}_3\text{H}_3\text{Cl}_2)$ . See text.

C<sub>3</sub>H<sub>3</sub>Cl to form C<sub>3</sub>H<sub>3</sub>Cl<sub>2</sub>. The system rapidly evolves to contain nearly equal concentrations of C<sub>3</sub>H<sub>3</sub>Cl<sub>2</sub> and C<sub>3</sub>H<sub>3</sub> radicals. Further evolution of the resulting system is driven by three key reactions: (1) self-reaction of C<sub>3</sub>H<sub>3</sub>Cl<sub>2</sub> radicals, (2) the cross-reaction between the C<sub>3</sub>H<sub>3</sub>Cl<sub>2</sub> and C<sub>3</sub>H<sub>3</sub> radicals, and (3) self-reactions of C<sub>3</sub>H<sub>3</sub> radicals. The kinetic model contains the reactions Cl + C<sub>3</sub>H<sub>3</sub>Cl and C<sub>3</sub>H<sub>3</sub>Cl<sub>2</sub> + C<sub>3</sub>H<sub>3</sub>Cl<sub>2</sub> for which we determined reaction rate coefficients in the Cl<sub>2</sub>/C<sub>3</sub>H<sub>3</sub>Cl experiments (Table 1), where complications from competing reactions are minimal. We fixed  $k(\text{Cl} + \text{C}_3\text{H}_3\text{Cl})$  and  $k(\text{C}_3\text{H}_3\text{Cl}_2 + \text{C}_3\text{H}_3\text{Cl}_2)$  to the values listed in Table 1. The kinetic model does not contain the reactions Cl + C<sub>3</sub>H<sub>3</sub>Cl<sub>2</sub>, Cl + Cl, and Cl + C<sub>3</sub>H<sub>3</sub> because initial results indicate that the chlorine atoms react to depletion during the first 50 ± 30 μs after the photolysis event, thus rendering these reactions unimportant.

Figure 4 shows the relative influence of the cross-reaction C<sub>3</sub>H<sub>3</sub>Cl<sub>2</sub> + C<sub>3</sub>H<sub>3</sub> upon the time-resolved absorption traces measured at 242 nm in the two different chemical reaction systems. The traces were obtained under nearly the same reaction conditions (298 K and 660 Pa). At short times, both traces have nearly the same maximum concentration of C<sub>3</sub>H<sub>3</sub>Cl<sub>2</sub> radicals. Signal trace A, comprised of solid squares, shows the absorption decay initiated by photolyzing molecular chlorine at 351 nm in the presence of C<sub>3</sub>H<sub>3</sub>Cl. This simple, relatively

clean reaction system (see Table 1) provides a direct measure of the rate coefficient,  $k(\text{C}_3\text{H}_3\text{Cl}_2 + \text{C}_3\text{H}_3\text{Cl}_2)$ . Signal trace B, depicted with crosses, shows the absorption decay that follows the 193 nm photolysis of propargyl chloride. Like signal trace A, the decay of trace B reflects the activity of the self-reaction C<sub>3</sub>H<sub>3</sub>Cl<sub>2</sub> + C<sub>3</sub>H<sub>3</sub>Cl<sub>2</sub>, but the decay of trace B is further accelerated by the activity of the cross-reaction with propargyl radicals, C<sub>3</sub>H<sub>3</sub> + C<sub>3</sub>H<sub>3</sub>Cl<sub>2</sub> (see Table 2).

To derive the  $k(\text{C}_3\text{H}_3 + \text{C}_3\text{H}_3\text{Cl}_2)$  rate coefficient from signal trace B of Figure 4, we require knowledge of  $k(\text{C}_3\text{H}_3 + \text{C}_3\text{H}_3)$ . Propargyl radicals absorb strongly at 332.5 nm and do not absorb at 242 nm.<sup>1,17,18</sup> In a separate study we used procedures similar to those described here and measured the time-resolved decays of C<sub>3</sub>H<sub>3</sub> radicals at 332.5 nm following photolysis of allene, C<sub>3</sub>H<sub>3</sub>Cl, and C<sub>3</sub>H<sub>3</sub>Br with 193 nm light. Initially, the simplest second-order analysis of each data set constrained  $k(\text{C}_3\text{H}_3 + \text{C}_3\text{H}_3)$  to  $\leq (6.6 \pm 0.8) \times 10^{-11}$  cm<sup>3</sup> molecule<sup>-1</sup> s<sup>-1</sup>. This apparent  $k(\text{C}_3\text{H}_3 + \text{C}_3\text{H}_3)$  represented the upper limit, since for each precursor a cross-reaction with a companion radical, e.g., C<sub>3</sub>H<sub>5</sub> (allyl), C<sub>3</sub>H<sub>3</sub>Cl<sub>2</sub>, or C<sub>3</sub>H<sub>3</sub>Br<sub>2</sub>, accelerates the apparent  $k(\text{C}_3\text{H}_3 + \text{C}_3\text{H}_3)$ . Our computational models of the allene photolysis data (which monitored C<sub>3</sub>H<sub>3</sub> decays) indicate that  $k'(\text{C}_3\text{H}_3 + \text{C}_3\text{H}_3) = (4.4 \pm 1.4) \times 10^{-11}$  cm<sup>3</sup> molecule<sup>-1</sup> s<sup>-1</sup> (primed rate coefficients do not contain the uncertainty of the absorption cross section).<sup>1</sup> For the kinetic model of the reactions following C<sub>3</sub>H<sub>3</sub>Cl photolysis, the knowledge of  $k(\text{C}_3\text{H}_3\text{Cl}_2 + \text{C}_3\text{H}_3\text{Cl}_2)$  allowed us to fit directly the C<sub>3</sub>H<sub>3</sub> decay data and to determine  $k'(\text{C}_3\text{H}_3 + \text{C}_3\text{H}_3) = (4.2 \pm 0.9) \times 10^{-11}$  cm<sup>3</sup> molecule<sup>-1</sup> s<sup>-1</sup>.<sup>1</sup> By constraining  $k'(\text{C}_3\text{H}_3 + \text{C}_3\text{H}_3)$  to range between the rates obtained from the allene and C<sub>3</sub>H<sub>3</sub>Cl data at 332.5 nm, we modeled the C<sub>3</sub>H<sub>3</sub>Br data observed at 242 nm and obtained trial values of  $k(\text{C}_3\text{H}_3\text{Br}_2 + \text{C}_3\text{H}_3\text{Br}_2)$  and other rate coefficients (vide infra). These trial rate coefficients were adopted and used to fit the C<sub>3</sub>H<sub>3</sub>Br photolysis data observed at 332.5 nm (C<sub>3</sub>H<sub>3</sub> decays) to obtain a  $k'(\text{C}_3\text{H}_3 + \text{C}_3\text{H}_3)$ . The weighted average of the three  $k'(\text{C}_3\text{H}_3 + \text{C}_3\text{H}_3)$  gave a new  $k(\text{C}_3\text{H}_3 + \text{C}_3\text{H}_3)$ . This recursive cycle of fitting the C<sub>3</sub>H<sub>3</sub>Br data (at 242 and 332.5 nm) was repeated once, and all rate coefficients converged (Table 3). These determinations yielded the final rate coefficient,  $k(\text{C}_3\text{H}_3 + \text{C}_3\text{H}_3) = (4.3 \pm 0.6) \times 10^{-11}$  cm<sup>3</sup> molecule<sup>-1</sup> s<sup>-1</sup> at 298 K, where the stated uncertainty is two standard deviations and includes the uncertainty of the absorption cross section.<sup>1</sup>

By using the final (converged) rate coefficient,  $k(\text{C}_3\text{H}_3 + \text{C}_3\text{H}_3)$ , we refit the 242 nm decay data observed from the photolysis of C<sub>3</sub>H<sub>3</sub>Cl by adjusting only the cross-reaction rate coefficient. This procedure yielded  $k(\text{C}_3\text{H}_3 + \text{C}_3\text{H}_3\text{Cl}_2) = (7 \pm 6) \times 10^{-11}$  cm<sup>3</sup> molecule<sup>-1</sup> s<sup>-1</sup>. The parallel study, which fitted the propargyl radical decay data at 332.5 nm, indicated a second,



**TABLE 3: Kinetic Model and Derived Rate Coefficients That Interpret the Signal Traces Produced by 193 nm Photolysis of C<sub>3</sub>H<sub>3</sub>Br in N<sub>2</sub> Buffer at 298 K<sup>a</sup>**

reaction	rate coefficient, <sup>b</sup> cm <sup>3</sup> molecule <sup>-1</sup> s <sup>-1</sup>	comments
C <sub>3</sub> H <sub>3</sub> Br + 193 nm → C <sub>3</sub> H <sub>3</sub> + Br	$f_{1a} = 0.5$	branching ratio adopted from ref 3
C <sub>3</sub> H <sub>3</sub> Br + 193 nm → C <sub>3</sub> H <sub>2</sub> + HBr	$f_{1b} = 0.5$	branching ratio adopted from ref 3
C <sub>3</sub> H <sub>3</sub> Br + Br → C <sub>3</sub> H <sub>3</sub> Br <sub>2</sub>	$(2 \pm 1) \times 10^{-12}$	fitted value of this study
C <sub>3</sub> H <sub>3</sub> + Br → C <sub>3</sub> H <sub>3</sub> Br	$6.5 \times 10^{-11}$	unadjusted rate from ref 1
C <sub>3</sub> H <sub>3</sub> + C <sub>3</sub> H <sub>3</sub> → C <sub>6</sub> H <sub>6</sub>	$4.3 \times 10^{-11}$	unadjusted rate from ref 1
C <sub>3</sub> H <sub>3</sub> Br <sub>2</sub> + Br → products	$(8 \pm 4) \times 10^{-11}$	fitted value of this study
C <sub>3</sub> H <sub>3</sub> Br <sub>2</sub> + C <sub>3</sub> H <sub>3</sub> Br <sub>2</sub> → products	$(1.7 \pm 1.1) \times 10^{-11}$	fitted value of this study
C <sub>3</sub> H <sub>3</sub> + C <sub>3</sub> H <sub>3</sub> Br <sub>2</sub> (+M) → products	$(2 \pm 1.8) \times 10^{-11}$	fitted value of this study
C <sub>3</sub> H <sub>2</sub> + C <sub>3</sub> H <sub>3</sub> Br <sub>2</sub> → products	$4 \times 10^{-11}$	unadjusted value (see text)
C <sub>3</sub> H <sub>2</sub> + Br → C <sub>3</sub> H <sub>2</sub> Br	$4 \times 10^{-11}$	unadjusted value (see text)
C <sub>3</sub> H <sub>3</sub> + C <sub>3</sub> H <sub>2</sub> → products	$5 \times 10^{-11}$	unadjusted value (see text)
C <sub>3</sub> H <sub>2</sub> + C <sub>3</sub> H <sub>2</sub> → products	$5 \times 10^{-11}$	unadjusted value (see text)
C <sub>3</sub> H <sub>2</sub> + C <sub>3</sub> H <sub>3</sub> Br → products	$5 \times 10^{-12}$	unadjusted value (see text)

<sup>a</sup> The experiments monitored the C<sub>3</sub>H<sub>3</sub>Br<sub>2</sub> (tentatively assigned as 1,2-dibromoallyl) radical concentration at 242 nm. <sup>b</sup> Uncertainties denote two standard deviations including the propagated uncertainty of the absorption cross section.

separate determination,  $k(\text{C}_3\text{H}_3 + \text{C}_3\text{H}_3\text{Cl}_2) = (7 \pm 4) \times 10^{-11}$  cm<sup>3</sup> molecule<sup>-1</sup> s<sup>-1</sup>, that is in agreement with the first.<sup>1</sup> The relative imprecision of both determinations of  $k(\text{C}_3\text{H}_3 + \text{C}_3\text{H}_3\text{Cl}_2)$  arises from the similar magnitudes of  $k(\text{C}_3\text{H}_3 + \text{C}_3\text{H}_3)$ ,  $k(\text{C}_3\text{H}_3 + \text{C}_3\text{H}_3\text{Cl}_2)$ , and  $k(\text{C}_3\text{H}_3\text{Cl}_2 + \text{C}_3\text{H}_3\text{Cl}_2)$  and because the initial populations of C<sub>3</sub>H<sub>3</sub> and C<sub>3</sub>H<sub>3</sub>Cl<sub>2</sub> radicals are nearly equal.

While conducting the numeric modeling of the decay data observed at 242 nm, we found that the derived rate coefficients, their uncertainties, and the fidelity of the calculated decays to the data were fairly sensitive to the chosen value of  $k(\text{C}_3\text{H}_3 + \text{C}_3\text{H}_3)$ . Morter et al.<sup>2</sup> have reported a  $k(\text{C}_3\text{H}_3 + \text{C}_3\text{H}_3)$  at 298 K that is about 2.5 times faster than our chosen rate coefficient (Table 2). When we attempted to use this elevated  $k(\text{C}_3\text{H}_3 + \text{C}_3\text{H}_3)$ , we found that our model could not reproduce the 242 nm signal traces of the C<sub>3</sub>H<sub>3</sub>Cl data set.

**Rate Coefficients in the Propargyl Bromide System.** Table 3 summarizes the kinetic model used to fit the rise and decay of C<sub>3</sub>H<sub>3</sub>Br<sub>2</sub> formed by the 193 nm photolysis of mixtures containing propargyl bromide and N<sub>2</sub> buffer. During each experiment the transient absorbance was monitored at 242 nm. The propargyl bromide partial pressure was set between 2 and 6 Pa, and N<sub>2</sub> buffer was added to stabilize the total pressure at 605 Pa (4.6 Torr). According to fits of the kinetic model, the typical photolysis event dissociated about 3% of the irradiated propargyl bromide.

Rate coefficients for  $k(\text{Br} + \text{C}_3\text{H}_3\text{Br})$ ,  $k(\text{C}_3\text{H}_3\text{Br}_2 + \text{C}_3\text{H}_3\text{Br}_2)$ , and  $k(\text{C}_3\text{H}_3 + \text{C}_3\text{H}_3\text{Br}_2)$  were extracted by fitting experiments that generated 100 point signal traces of 1, 2, 10, and 20 ms duration. Table 3 lists the average rate coefficients and their uncertainties. As mentioned above, the kinetic model used during these determinations also incorporated the reaction rate coefficients  $k(\text{C}_3\text{H}_3 + \text{C}_3\text{H}_3)$  and  $k(\text{Br} + \text{C}_3\text{H}_3)$ , which are reported elsewhere.<sup>1</sup> Absorption due to the C<sub>3</sub>H<sub>2</sub> carbene diminishes rapidly and is unimportant by  $t \approx 400$  μs. To simulate the decay of C<sub>3</sub>H<sub>2</sub>, we added a set of cross-reactions between C<sub>3</sub>H<sub>2</sub> carbene and other species (Table 3). Since C<sub>3</sub>H<sub>3</sub>Br is in large excess, the rate coefficient  $k(\text{C}_3\text{H}_2 + \text{C}_3\text{H}_3\text{Br})$  governs the apparent C<sub>3</sub>H<sub>2</sub> loss rate. Modeling showed that our choices of cross-rate coefficients contribute some uncertainty to the fit of  $k(\text{Br} + \text{C}_3\text{H}_3\text{Br})$  but have negligible influence upon  $k(\text{C}_3\text{H}_3\text{Br}_2 + \text{C}_3\text{H}_3\text{Br}_2)$  and  $k(\text{C}_3\text{H}_3 + \text{C}_3\text{H}_3\text{Br}_2)$ , which are determined by data observed at longer reaction times.

Figure 2 shows a plot of the absorbance data measured at 242 nm and the fit that extracts one individual rate for  $k(\text{C}_3\text{H}_3\text{Br}_2 + \text{C}_3\text{H}_3\text{Br}_2)$  by fitting the signal decay. Fits of data obtained

at early times ( $t < 2$  ms) found the radical production rate  $k(\text{Br} + \text{C}_3\text{H}_3\text{Br})$ . During the fitting process we found that the cross-reaction rate coefficient  $k(\text{C}_3\text{H}_3 + \text{C}_3\text{H}_3\text{Br}_2)$  was determined principally by data observed at times greater than 10 ms after the photolysis pulse.

**Computational Results Leading to the Reaction Energy Surface of Cl + Propargyl Chloride.** To interpret the experimental data, we need to understand the reaction energy surface that governs halogen atom addition to propargyl halides. The construction of this energy surface for reaction 4 requires knowledge of the enthalpy of formation,  $\Delta_f H_0^\circ$ , for each reactant, incipient radical, transition-state structure, secondary radical generated by isomerization, and stable product. In all, the energy surface for reaction 4 requires consideration of about 14 species of which most have no known thermochemistry. To estimate the unknown  $\Delta_f H_0^\circ$ 's, we performed a series of ab initio calculations on the incipient radicals and reaction products formed by adding a chlorine atom to propargyl chloride. The initial results stimulated a broader study of the isomerization energy barriers within several C<sub>3</sub> radicals, which is reported elsewhere.<sup>30</sup> Initially, we performed UHF//6-31G\* calculations to find the stable structures of the adducts. To find the minimum energy conformer of each radical isomer, we mapped the energy of its internal rotations by computing a UHF//6-31G\* optimized structure every 15° along each internal rotation coordinate. These minimum energy conformer structures were further refined with a series of G2 calculations as implemented by the Gaussian 94 program. These results yielded the G2 energy of each structure,  $H^{G2}$ , which were used to derive  $\Delta_f H_0^\circ$  for species of previously unknown thermochemistry.

Table 4 lists enthalpies of formation,  $\Delta_f H_0^\circ$  of the reactants, products, and the radical intermediates associated with the reaction of chlorine with propargyl chloride (reaction 4). To maintain consistent energy relationships, thermochemical enthalpies involved in reaction 4 were computed using the experimentally known  $\Delta_f H_0^\circ(\text{propyne})$ , when possible. Key among these is  $\Delta_f H_0^\circ(\text{allene})$ , which we derived by combining  $\Delta_f H_0^\circ(\text{propyne})$  with the experimentally determined heat of isomerization.<sup>31,32</sup>

The listed  $\Delta_f H_0^\circ(\text{calc})$ 's were computed using the results of G2 calculations and thus were computed assuming that each species contains only harmonic oscillators and rigid rotors. To compensate for inaccuracies originating from spin contamination

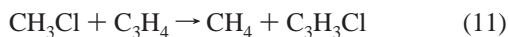
**TABLE 4: Experimental Data and G2 Computational Results Used To Estimate the Relative Energies of the Species Involved in Reactions 4 and 16**

species	$H_0^{G2}$ , hartree <sup>a</sup>	$H_{298.15}^{G2}$ , hartree <sup>a</sup>	$\Delta_f H_0^{\circ}(\text{calc})$ , kJ mol <sup>-1</sup>	$\Delta_f H_{298.15}^{\circ}(\text{calc})$ , kJ mol <sup>-1</sup>	$\Delta_f H_0^{\circ}(\text{expt})$ , kJ mol <sup>-1</sup>	$\Delta_f H_{298.15}^{\circ}(\text{expt})$ , kJ mol <sup>-1</sup>
(E)-1,2-dichloroallyl cation ( $C_s$ )	-1 035.011 566	-1 035.005 102	(909 ± 4) <sup>b</sup>			
(E)-1,2-dichloroallyl radical ( $C_s$ )	-1 035.311 626	-1 035.304 856	117 ± 3	110 ± 3		
(Z)-1,2-dichloroallyl radical ( $C_s$ )	-1 035.310 127	-1 035.303 369	121 ± 3	114 ± 3		
(E,E)-1,3-dichloroallyl radical ( $C_{2v}$ )	-1 035.308 817	-1 035.302 087	125 ± 3	117 ± 3		
(E,Z)-1,3-dichloroallyl radical ( $C_s$ )	-1 035.313 514	-1 035.306 715	112 ± 3	105 ± 3		
(Z,Z)-1,3-dichloroallyl radical ( $C_{2v}$ )	-1 035.312 045	-1 035.305 078	116 ± 3	109 ± 3		
(E)-1,3-dichloro-1-propene-2-yl radical ( $C_s$ )	-1 035.269 721	-1 035.262 723	227.8 ± 1.7	221.1 ± 1.7		
(Z)-1,3-dichloro-1-propene-2-yl radical ( $C_s$ )	-1 035.269 477	-1 035.262 610	228.4 ± 1.7	221.4 ± 1.7		
2,3-dichloro-1-propene-1-yl radical	-1 035.268 913	-1 035.262 164	229.9 ± 1.7	222.6 ± 1.7		
allyl cation ( $C_{2v}$ )	-116.708 706	-116.703 913			[966 ± 4] <sup>c</sup>	
allyl radical ( $C_{2v}$ )	-117.005 896	-117.000 936			(182 ± 3) <sup>d</sup>	(171 ± 3) <sup>e</sup>
chloropropargyl radical ( $C_s$ )	-574.923 386	-574.917 499	316 ± 5	315 ± 4		
propargyl radical ( $C_{2v}$ )	-115.773 299	-115.768 062			(341 ± 4) <sup>d</sup>	(339 ± 4) <sup>e</sup>
2,3-dichloro-1-propene allene ( $D_{2d}$ )	-1 035.948 916	-1035.942 257	-36.9 ± 1.5	-25.1 ± 1.5		
chloroallene ( $C_s$ )	-116.417 840	-116.413 085			(195.9 ± 2.3) <sup>d</sup>	(188.3 ± 2.3) <sup>f</sup>
ethylene	-575.564 903	-575.559 454	178.6 ± 2.8	181.6 ± 2.8		
methane	-78.415 925				(192.5 ± 0.9) <sup>g</sup>	(184.5 ± 0.9) <sup>g</sup>
methyl chloride ( $C_{3v}$ )	-40.410 885				(-66.63 ± 0.3) <sup>h</sup>	
propargyl chloride ( $C_s$ )	-499.553 828	-575.556 910	185.3 ± 1.7	188.4 ± 1.7	(-73.94 ± 0.6) <sup>h</sup>	
propene	-575.562 373				(60.92 ± 0.5) <sup>h</sup>	(20.0 ± 0.5) <sup>i</sup>
vinyl chloride	-117.645 074				(35.0 ± 0.5) <sup>i</sup>	
Cl	-537.568 284				(30.57 ± 2.1) <sup>h</sup>	
	-459.677 966 <sup>k</sup>	-459.675 605 <sup>k</sup>			(119.621 ± 0.006) <sup>j</sup>	(121.301 ± 0.008) <sup>j</sup>

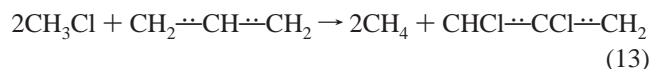
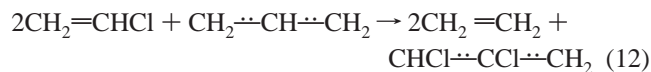
<sup>a</sup> 1 hartree = 2625.43 kJ mol<sup>-1</sup>. <sup>b</sup> Based on  $IE_a(C_3H_3Cl_2) = 8.17 \pm 0.02$  eV derived from  $H_0^{G2}$ 's and adjusted by  $IE_a(C_3H_5)$ . See text. <sup>c</sup> Derived using  $\Delta_f H_{298.15}^{\circ}(\text{expt, allyl})$  and  $IE_a(C_3H_5) = 8.13 \pm 0.02$  eV from ref 36. <sup>d</sup> Computed using the  $\Delta_f H_{298.15}^{\circ}(\text{expt})$ , the heat function derived from  $H_0^{G2} - H_{298.15}^{G2}$ , and standard states of ref 50. <sup>e</sup> From ref 35. <sup>f</sup> Computed using  $\Delta_f H_{298.15}^{\circ}(\text{expt, propyne})$  and the enthalpy of isomerization that is reported in ref 31 and reanalyzed in ref 32. <sup>g</sup> From ref 51. <sup>h</sup> From ref 52. <sup>i</sup> Computed using  $\Delta_f H_{298.15}^{\circ}(\text{expt, propyne})$  from ref 53 and the heat correction from ref 54. <sup>j</sup> From ref 53. <sup>k</sup> A correction of  $E = -0.001\ 338\ 2$  hartree is added to account for the spin-orbit energy. <sup>l</sup> From ref 50.

(which for all radicals did not exceed  $S^2 = 0.762$ , as compared to the ideal  $S^2 = 0.75$ , after projection of the highest spin contaminant) and correlation errors, we calculated  $\Delta_f H_0^{\circ}(\text{calc})$  by combining the G2 energies,  $H_0^{G2}$ , and experimentally known heats of formation (Table 4) in reaction schemes. These standard methods for estimating  $\Delta_f H_0^{\circ}$  are discussed elsewhere in greater detail.<sup>33,34</sup>

We computed  $\Delta_f H_0^{\circ}(\text{calc})$  for the 2,3-dichloro-1-propene-1-yl and 1,3-dichloro-1-propene-2-yl radicals using isogyric reaction schemes based on reaction 4. We computed  $\Delta_f H_0^{\circ}(C_3H_3Cl)$  for chloroallene, propargyl chloride, and 2,3-dichloropropene by averaging the values obtained for isodesmic reactions involving stable species of known thermochemistry, e.g.,



In a similar fashion we computed  $\Delta_f H_0^{\circ}$  for the 1,3-dichloroallyl and 1,2-dichloroallyl radicals with isodesmic reactions involving the allyl radical, e.g.,



Our computations used  $\Delta_f H_0^{\circ}(\text{expt, allyl radical})$  and  $\Delta_f H_0^{\circ}(\text{expt, -$

propargyl radical), which we calculated using values of  $\Delta_f H_{298.15}^{\circ}(\text{expt})$  recommended in the recent review by Tsang.<sup>35</sup>

In the Discussion we also account for the optical spectrum by assigning the upper state as a Rydberg state of the 1,2-dichloroallyl radical. Arguments supporting this assignment are strengthened by knowledge of the ionization energies of the allyl and 1,2-dichloroallyl radicals. Table 2 lists the G2 energies of the allyl cation and 1,2-dichloroallyl cation ground-state structures. The G2 energies predict that the first adiabatic ionization energy from the  $\tilde{X}^2A_2$  state of allyl radical is  $IE_a^{G2}(C_3H_5) = 8.09$  eV. For comparison, photoelectron experiments obtained  $IE_a(C_3H_5) = 8.13 \pm 0.02$  eV.<sup>36</sup> For the 1,2-dichloroallyl radical the G2 energies predict  $IE_a^{G2}(C_3H_3Cl_2) = 8.17$  eV. Using the correction implied by the allyl radical results, we predict  $IE_a(C_3H_3Cl_2) = 8.21 \pm 0.02$  eV. Table 2 lists  $\Delta_f H_0^{\circ}$  computed using the estimated  $IE_a$  of the 1,2-dichloroallyl radical.

## Discussion

### Reactive Pathways Available to Cl + Propargyl Chloride.

Figure 5 diagrams the relative energies of the reactants and energetically accessible products via the addition reaction of Cl and propargyl chloride. Figure 5 also shows the structure of each transient species. This diagram was constructed using the experimentally and computationally derived values of  $\Delta_f H_0^{\circ}$  listed in Table 4. The energy of each product channel (at 0 K), relative to the reactants, is shown in parentheses. Figure 5 shows only the energies and structures of the most stable radical isomers. We cannot rule out the existence of mechanistic details that will lead to the production of the less stable geometric



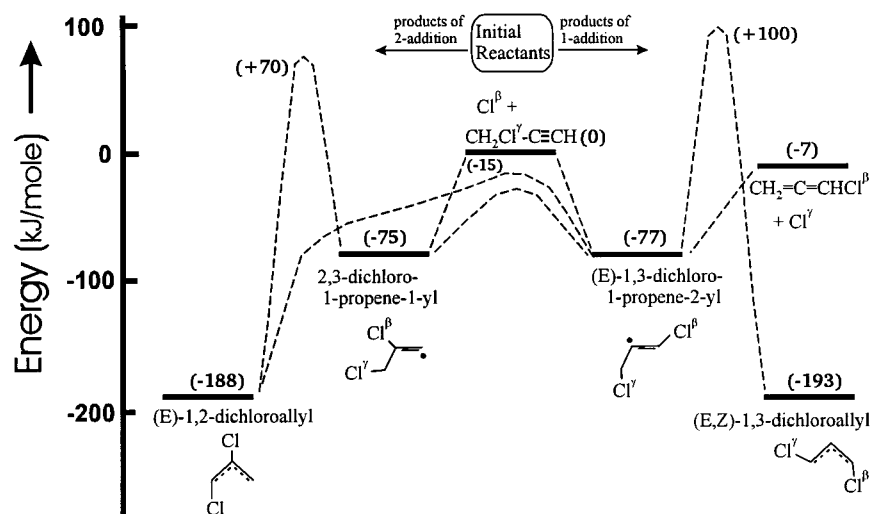
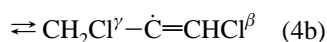
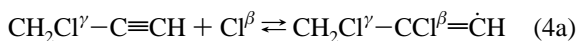


**Figure 5.** Energy diagram of the reactants, radical intermediates, and products that are energetically accessible during the reaction of Cl + propargyl chloride. The values listed in parentheses are the energies (in  $\text{kJ mol}^{-1}$ ) of the products with reference to the reactants ( $\text{Cl}^\beta + \text{CH}_2\text{Cl}^\gamma\text{C}\equiv\text{CH}$ ) at 0 K. Dashed lines indicate the isomerization paths involving shifts of a hydrogen or a chlorine atom between the carbons. The energy of each isomerization barrier, relative to the energy of the reactants, is listed in  $\text{kJ mol}^{-1}$ . See text and Table 5.

isomers. Nevertheless, Figure 5 shows a good thermochemical description of the reaction surface, since our calculations found that the  $\Delta_f H_0^\circ(\text{calc})$ 's among analogous isomers differ by 1–13  $\text{kJ mol}^{-1}$ .

Figure 5 also diagrams the isomerization barriers associated with a shift of a hydrogen or a chlorine atom among the carbons. Each isomerization energy barrier was computed from the average of the energy differences between each relevant, optimized, stationary transition-state structure and the initial and final radical structures. These energies were computed with a QCISD(T)/6-311+G\*\*//QCISD/6-31+G\*\* procedure, and the calculations include the appropriate zero-point vibrational energy contributions. A full description of the computational research that determined these transition structures is reported elsewhere.<sup>30</sup>

The ab initio calculations predict that the energy barriers impeding chlorine atom addition at the center and acetylenic carbons on propargyl chloride are negligibly small.<sup>30</sup> Addition onto the center carbon forms the vinylic structure, 2,3-dichloro-1-propene-1-yl radical. Addition onto the end carbon of the acetylene group forms the vinylic structure, 1,3-dichloro-1-propene-2-yl radical. Of course, both incipient vinyl radicals may undergo reverse reaction and re-form the initial products. Thus, we restate reaction 4 with the equations



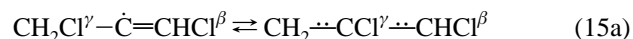
One unimolecular process is available to the 2,3-dichloro-1-propene-1-yl radicals formed through reaction 4a. When a chlorine atom is transferred from the center carbon to the end-carbon radical site, the 2,3-dichloro-1-propene-1-yl radical may isomerize into a 1,3-dichloro-1-propene-2-yl radical, e.g.,



The barriers separating the 2,3-dichloro-1-propene-1-yl and 1,3-dichloro-1-propene-2-yl radical isomers are low ( $\sim 45 \text{ kJ mol}^{-1}$ ), and both vinylic  $\text{C}_3\text{H}_3\text{Cl}_2$  radicals are of nearly equal energy (Table 4 and Figure 5). Thus, the forward and reverse processes of reaction 14 should have comparable rates. Under certain

conditions an equilibrium may exist between these isomers. We might expect both incipient vinyl radicals to isomerize into more stable allyl radicals; however, such isomerizations cannot occur through transfer of a hydrogen from the chloromethyl group to a radical site. Such isomerization processes are inhibited by large ( $> 145 \text{ kJ mol}^{-1}$ ) energy barriers (Figure 5).<sup>30</sup>

In addition to reaction -14, two other unimolecular processes deplete the 1,3-dichloro-1-propene-2-yl radical population: (a) the chloromethyl group may transfer its chlorine to the center carbon, forming the 1,2-dichloroallyl radical, and (b) the chloromethyl group may undergo C–Cl bond scission, producing a chloroallene and a chlorine atom, e.g.,



Reaction 15a forms 1,2-dichloroallyl radicals. By using canonical transition-state theory formalism<sup>37–40</sup> and computer code developed at NIST,<sup>41</sup> we estimated the unimolecular rate parameters for reactions 15a and -15a at the high-pressure limit. The calculations predict forward and reverse Arrhenius factors ( $A^{15a} \approx 3.4 \times 10^{12} \text{ s}^{-1}$  and  $A^{-15a} \approx 3.7 \times 10^{13} \text{ s}^{-1}$ ) and activation energies ( $E_a^{15a} = 64.4 \text{ kJ mol}^{-1}$  and  $E_a^{-15a} = 164.1 \text{ kJ mol}^{-1}$ ). (Here, we ignore the temperature variances of the predicted unimolecular rate parameters because an explicit accounting would not affect conclusions regarding the reaction mechanism.) The large difference between the forward and reverse activation energies renders the isomerization of 1,3-dichloro-1-propene-2-yl radicals into 1,2-dichloroallyl radicals as effectively irreversible. The 1,2-dichloroallyl radicals, formed by reaction 15a, will persist until depleted through bimolecular reactions.

Reaction 15b produces chloroallene and regenerates a chlorine atom. The Arrhenius parameters for both C–Cl<sup>β</sup> and C–Cl<sup>γ</sup> bond scissions are expected to be large ( $A \approx 10^{14} \text{ s}^{-1}$ ) and nearly equal. In the 1,3-dichloro-1-propene-2-yl radical the activation energy barrier impeding elimination of Cl<sup>γ</sup> (reaction 15b) is  $\sim 7 \text{ kJ mol}^{-1}$  lower than the activation energy barrier for elimination of Cl<sup>β</sup> (reaction -4b). Thus, reaction 15b is an important depletion channel for the 1,3-dichloro-1-propene-2-yl radical

population, but since this reaction produces a chlorine atom, its effects on the observed kinetics of 1,2-dichloroallyl are masked.

**Spectrum of the 1,2-Dichloroallyl Radical.** The end-product data and ab initio results indicate that the 1,2-dichloroallyl radical is the only radical remaining after the unimolecular processes (reactions 14 and 15) have been completed. Thus, we assign the optical spectrum and kinetic data as properties of the 1,2-dichloroallyl radical. This assignment is also consistent with the spectroscopic data known for the allyl radical. Between 408 and 241 nm the allyl ( $\tilde{X}^2A_2$ ) radical exhibits spectra from four upper electronic states.<sup>42–47</sup> Of these, the state of the 1,2-dichloroallyl radical that corresponds to the  $\tilde{C}[2^2B_1(3p)] \leftarrow \tilde{X}^2A_2$  transition of the allyl radical seems the most likely to account for the absorption strength of 1,2-dichloroallyl radical.

In the allyl radical the  $\tilde{C}[2^2B_1(3p)] \leftarrow \tilde{X}^2A_2$  transition absorbs strongly between 210 and 230 nm.<sup>43,48</sup> Its origin band corresponds to the absorption maximum and appears at 248 nm. Because this upper state has strong Rydberg character,<sup>49</sup> chlorine substitution may not change its structure substantially in the 1,2-chloroallyl radical. Therefore, we may estimate the energy of the corresponding origin band in the 1,2-dichloroallyl radical by shifting the origin band in the allyl radical spectrum ( $\nu_{00} = 40\,305\text{ cm}^{-1}$ ) by adding in the difference between the ionization energies of allyl and 1,2-chloroallyl radicals ( $IE_a(C_3H_3Cl_2) - IE_a(C_3H_5) = 0.08\text{ eV}$  (Table 4)). As an approximation, we ignore the small shift in the quantum defect induced by chlorine substitution. This procedure predicts that the  $\tilde{C}(3p) \leftarrow \tilde{X}$  origin band of 1,2-dichloroallyl radical should appear around  $\sim 244\text{ nm}$  ( $\nu_{00} \approx 40\,950\text{ cm}^{-1}$ ). Since the absorption maximum of the present spectrum appears at 240 nm (Figure 1), we conclude that the observed spectrum is consistent with the assignment of the spectral carrier as the 1,2-dichloroallyl radical.

**Interpretation of the Experimental Measurements.** With reference to the energy diagram (Figure 5), we can rationalize the relative abundances of the photolysis products and the temporal growth of the CRD absorbance signal. Referenced to the  $C_3$  product yield, the GC–MS analysis found chloroallene (75%), 2,3-dichloro-1-propene (24%), and 1,3-dichloro-1-propene (<1%). Chloroallene may arise only through reaction 15b. The 2,3-dichloro-1-propene may evidence (a) the production of 1,2-dichloroallyl radicals by reaction 15a, (b) the production of 2,3-dichloro-1-propene-1-yl radicals by reaction 4a, or (c) the sum of both reactions. The 1,3-dichloro-1-propene may arise only from the residual 1,3-dichloro-1-propene-2-yl radicals, and its sparse abundance indicates that very little 1,3-dichloro-1-propene-2-yl radical persists at long reaction times.

To explain these data, we postulate that the incipient ensemble of  $C_3H_3Cl_2$  radicals formed by reaction 4 is not at thermal equilibrium. This postulate is reasonable because each incipient  $C_3H_3Cl_2$  radical formed contains  $\geq 75\text{ kJ mol}^{-1}$  internal energy. Because this internal energy is  $\sim 30\text{ kJ mol}^{-1}$  greater than the isomerization barrier separating 2,3-dichloro-1-propene-1-yl and 1,3-dichloro-1-propene-2-yl radicals, reaction 14 rapidly establishes an equilibrium between these isomers. Furthermore, both barriers of reaction 15 lie at least  $7\text{ kJ mol}^{-1}$  below the energy of the  $C_3H_3Cl_2$  ensemble. As reaction 15 rapidly proceeds, forming Cl, chloroallene, and 1,2-dichloroallyl radicals, reaction 14 maintains an equilibrium between the vinylic isomers until the entire ensemble of 2,3-dichloro-1-propene-1-yl and 1,3-dichloro-1-propene-2-yl radicals is depleted. Since the Arrhenius factors of reactions 14 and 15 are greater than  $10^{12}\text{ s}^{-1}$ , the unimolecular decomposition of  $C_3H_3Cl_2$  is complete on a time scale that is short compared to collisional relaxation. The 1,2-

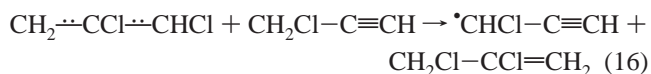
dichloroallyl radical population relaxes to the ambient temperature and persists until it is depleted by bimolecular reactions.

Reverse reaction –15a may account for the trace of 1,3-dichloro-1-propene observed in the end products. Since reaction 14 maintains equilibrium between the vinylic isomers, we expect a similar trace amount of 2,3-dichloro-1-propene-1-yl radical to persist at long reaction times and contribute to the fraction of 2,3-dichloro-1-propene observed in the end products. However, this trace can account for only a small fraction of the total 2,3-dichloro-1-propene detected.

In this view, 1,2-dichloroallyl radicals produce the transient CRDS absorption signal observed during this study at 240 nm. To our CRDS apparatus, which can only detect processes that change on time scales greater than  $\sim 2\text{ }\mu\text{s}$ , unimolecular reactions 14 and 15 are undetectable. However, CRDS does measure the concentration of 1,2-dichloroallyl radical, and the absorption increase (Figure 2a) provides a direct determination of  $k(\text{Cl} + C_3H_3Cl)$ . Since both vinylic isomer populations evolve together in equilibrium, the observed rate coefficient  $k(\text{Cl} + C_3H_3Cl)$  is equivalent to the rate coefficient of reaction 4.

The rate coefficients  $k(C_3H_3Cl_2 + C_3H_3Cl_2)$  and  $k(C_3H_3Cl_2 + C_3H_3)$  are fundamental rate coefficients of 1,2-dichloroallyl radicals. Reaction 15b produces Cl atoms that react rapidly in the excess of propargyl chloride. The sequence of reactions 4 and 15b forms a null cycle (with respect to the Cl atom budget) that channels the initial concentration of photolytic chlorine atoms into a nearly equal concentration of 1,2-dichloroallyl radicals. This sequence maintains the accuracy of the determinations of  $\sigma_{240}(C_3H_3Cl_2)$ , which is essential for accurate determinations of  $k(C_3H_3Cl_2 + C_3H_3Cl_2)$ .

The GC–MS analysis of the photolysis products of propargyl chloride contained 2,3-dichloro-1-propene. Conceivably, 2,3-dichloro-1-propene is produced by a reaction of 1,2-dichloroallyl radicals with propargyl chloride:



Results of ab initio calculations estimate that reaction 16 is exothermic by  $\Delta_r H_{298.15}^\circ = -(70 \pm 6)\text{ kJ mol}^{-1}$ . Since we see no evidence of pseudo-first-order behavior with respect to propargyl chloride concentration, reaction 16, if active, must be very slow and hidden in the measurement uncertainty of  $k(C_3H_3Cl_2 + C_3H_3Cl_2)$ .

If we presume that reaction 16 is active, the relative abundance of the chloroallene and 2,3-dichloro-1-propene among the end products gives an approximate measure of the branching ratio of reaction 15. Their 3:1 abundance ratio implies the branching ratio coefficients  $f_{15a} \approx 0.25$  and  $f_{15b} \approx 0.75$ . These coefficients are valid if all products of reaction 15 were available for GC–MS analysis. Since chloroallene is a stable molecule, its GC–MS signal probably accounts for reaction 15b properly. In contrast, 1,2-dichloroallyl radicals may recombine and engage in a cross-reaction with propargyl radicals. Since these reactions may not produce 2,3-dichloro-1-propene, the GC–MS signal from 2,3-dichloro-1-propene probably provides an upper limit of the product fraction formed by reaction 15a and  $f_{15a} \geq 0.25$ .

In an earlier study we assigned the 2,3-dichloro-1-propene-1-yl radical as the carrier of the 240 nm CRDS signal.<sup>1</sup> This reassignment does not alter the rate coefficients derived during that study because the specific identity of the  $C_3H_3Cl_2$  isomer does not affect the kinetic equations used for the data analyses.

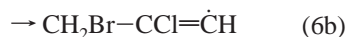
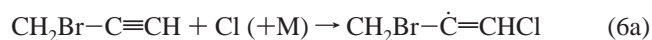
**Reactive Pathways of X (X = Cl, Br) + Propargyl Bromide.** For Br + propargyl bromide (reaction 6) the

substitution of chlorine by bromine will change the relative energies and production rates of the products; however, the overall reaction scheme should resemble the one found for  $\text{Cl} + \text{C}_3\text{H}_3\text{Cl}$ . The incipient radicals should rapidly isomerize, forming an equilibrium, and feed the channels leading to the final products, e.g.,



Because the relative energies of propargyl bromide and bromoallene are unknown, we are not certain that the 1,3-dibromo-1-propene-2-yl radical can undergo an exothermic reaction forming bromoallene and Br. However, the strong absorption signal indicates that the incipient radicals isomerize rapidly, forming 1,2-dibromoallyl radicals. Thus, the rate coefficients measured for  $\text{C}_3\text{H}_3\text{Br}_2$  are fundamental rate coefficients of the 1,2-dibromoallyl radical.

Kinetic schemes involving  $\text{Cl} +$  propargyl bromide should involve the reaction sequence



Thus, we assign the spectral carrier of  $\text{Cl} +$  propargyl bromide to the 1-chloro-2-bromoallyl radical formed by reaction 18a. Subsequent reactions by the bromine atom product of reaction 18b will generate 2,3-dibromoallyl radicals through reaction 6. The spectrum presented in Figure 1d has little contamination from this cycle because it contains signal observed at early times before the relatively slow bromine addition can generate appreciable concentrations of  $\text{C}_3\text{H}_3\text{Br}_2$ .

## Conclusion

Chlorine adds rapidly to propargyl chloride at the center and terminal unsaturated carbon atoms, forming vinylic  $\text{C}_3\text{H}_3\text{Cl}_2$  radicals. These radicals contain sufficient internal energy to establish equilibrium between their isomers. The 1,3-dichloro-1-propene-2-yl radical isomer rapidly transforms through two unimolecular processes: (1) isomerization forming 1,2-dichloroallyl radicals and (2) decomposition forming chloroallene and a chlorine atom. The persistent radical product, 1,2-dichloroallyl radical, exhibits an absorption spectrum that has an onset at 252 nm and extends to wavelengths shorter than 238 nm. By using cavity ring-down spectroscopy, we have measured the absorption cross section of the 1,2-dichloroallyl radical and determined the rate coefficients for its formation from  $\text{Cl} +$  propargyl chloride, its recombination reaction, and its reaction with the propargyl radical. Preliminary studies of the analogous reactions of chlorine and bromine with propargyl bromide give evidence that their reaction schemes are similar to those of  $\text{Cl} +$  propargyl chloride. The spectral carriers of these experiments are interpreted to arise from 1-chloro-2-bromoallyl and 1,2-dibromoallyl radicals, respectively.

**Acknowledgment.** We thank Dr. Jeffrey Manion for experimental assistance and for insightful discussions during the preparation of this manuscript. We thank Dr. Russell D. Johnson,

III and Dr. Carlos Gonzalez for assistance and advice with the ab initio calculations. We thank Dr. Thomas C. Allison for programming help with the numerical simulation software.

## References and Notes

- Atkinson, D. B.; Hudgens, J. W. *J. Phys. Chem. A* **1999**, *103*, 4242.
- Morter, C. L.; Farhat, S. K.; Adamson, J. D.; Glass, G. P.; Curl, R. F. *J. Phys. Chem.* **1994**, *98*, 7029.
- Slagle, I. R.; Gmurczyk, G. W.; Batt, L.; Gutman, D. *Symp. (Int.) Combust., [Proc.]* **1990**, *23*, 115.
- Slagle, I. R.; Gutman, D. *Symp. (Int.) Combust., [Proc.]* **1988**, *21*, 875.
- Fahr, A.; Hassanzadeh, P.; Laszlo, B.; Huie, R. E. *Chem. Phys.* **1997**, *215*, 59.
- Kaiser, E. W.; Wallington, T. J. *J. Phys. Chem.* **1996**, *100*, 9788.
- Kaiser, E. W. *Int. J. Chem. Kinet.* **1992**, *24*, 179.
- Atkinson, R.; Aschmann, S. M. *Int. J. Chem. Kinet.* **1985**, *17*, 33.
- DeMore, W. B.; Sander, S. P.; Golden, D. M.; Hampson, R. F.; Kurylo, M. J.; Howard, C. J.; Ravishankara, A. R.; Kolb, C. E.; Molina, M. J. *Chemical kinetics and photochemical data for use in stratospheric modeling. Evaluation number 12*; JPL Publication 97-4; Jet Propulsion Laboratory: Pasadena, CA, 1997.
- Atkinson, R.; Baulch, D. L.; Cox, R. A.; Hampson, R. F., Jr.; Rossi, M. J.; Kerr, J. A.; Troe, J. *J. Phys. Chem. Ref. Data* **1997**, *26*, 521.
- Atkinson, D. B.; Hudgens, J. W. *J. Phys. Chem. A* **1997**, *101*, 3901.
- Certain commercial materials and equipment are identified in this paper in order to adequately specify the experimental procedure. Such identification neither implies recommendation or endorsement by the National Institute of Standards and Technology nor does it imply that the material or equipment identified is the best available for the purpose.
- Nonlinear Levenberg-Marquardt fitting virtual instrument. Labview 4.0*; National Instruments Corporation: Austin, TX, 1994-1995.
- Miller, J. A.; Melius, C. F. *Combust. Flame* **1992**, *91*, 21.
- Braun, W. *Int. J. Chem. Kinet.* **1988**, *20*, 51.
- Frisch, M. J.; Trucks, G. W.; Schlegel, H. B.; Gill, P. M. W.; Johnson, B. G.; Robb, M. A.; Cheeseman, J. R.; Keith, T.; Petersson, G. A.; Montgomery, J. A.; Raghavachari, K.; Al-Laham, M. A.; Zakrzewski, V. G.; Ortiz, J. V.; Foresman, J. B.; Cioslowski, J.; Stefanov, B. B.; Nanayakkara, A.; Challacombe, M.; Peng, C. Y.; Ayala, P. Y.; Chen, W.; Wong, M. W.; Andres, J. L.; Replogle, E. S.; Gomperts, R.; Martin, R. L.; Fox, D. J.; Binkley, J. S.; Defrees, D. J.; Baker, J.; Stewart, J. P.; Head-Gordon, M.; Gonzalez, C.; Pople, J. A. *Gaussian 94*, revision D.4; Gaussian, Inc.: Pittsburgh, PA, 1995.
- Jacox, M. E.; Milligan, D. E. *Chem. Phys.* **1974**, *4*, 45.
- Ramsay, D. A.; Thistlethwaite, P. *Can. J. Phys.* **1966**, *44*, 1381.
- Seki, K.; Okabe, H. *J. Phys. Chem.* **1992**, *96*, 3345.
- Sun, W.; Yokoyama, K.; Robinson, J. C.; Suits, A. G.; Neumark, D. M. *J. Phys. Chem.* **1999**, *110*, 4363.
- Satyapal, S.; Bersohn, R. *J. Phys. Chem.* **1991**, *95*, 8004.
- Jacox, M. E. *J. Phys. Chem. Ref. Data* **1994**, *13* (461 pages).
- Jacox, M. E. *J. Phys. Chem. Ref. Data* **1998**, *27*, 115.
- Seburg, R. A.; Paterson, E. V.; Stanton, J. F.; McMahon, R. J. *J. Am. Chem. Soc.* **1997**, *119*, 5847.
- Stanton, J. F.; DePinto, J. T.; Seburg, R. A.; Hodges, J. A.; McMahon, R. J. *J. Am. Chem. Soc.* **1997**, *119*, 429.
- Propargyl chloride eluted from the GC column 4.34 min after sample injection. Samples of propargyl chloride that were illuminated with 193 nm laser light also eluted a strong peak 4.07 min after sample injection, which we assign as chloroallene. This eluent produced a mass spectrum with the relative abundances:  $m/z$  76 (9),  $m/z$  75 (2),  $m/z$  74 (27),  $m/z$  73 (4),  $m/z$  72 (1),  $m/z$  49 (1),  $m/z$  47 (3),  $m/z$  40 (4),  $m/z$  39 (100),  $m/z$  38 (23),  $m/z$  37 (25),  $m/z$  36 (8), and  $m/z$  35 (5). The relative abundance of  $m/z$  40 is unreliable because of a small amount of Ar contamination from leaked air.
- Hodges, J. T.; Looney, J. P.; van Zee, R. D. *Appl. Opt.* **1996**, *35*, 4112.
- Atkinson, D. B.; Hudgens, J. W. Chlorination Chemistry. 2. Ultraviolet Cavity Ring-down Spectroscopic Measurements and ab initio Calculations of Chlorine Atom Reactions with Allene. *J. Phys. Chem. A*, in press.
- Taylor, B. E. *Guide for the Use of the International System of Units (SI)*, 1995 ed.; National Institute of Standards and Technology: Gaithersburg, MD, 1995.
- Hudgens, J. W.; Gonzalez, C. Chlorination Chemistry. 4. Ab Initio Study of the Potential Energy Surface Governing Isomerization within the  $\text{C}_3\text{H}_3\text{Cl}_2$  Addition Complex Formed by Chlorine and Propargyl Chloride. Manuscript in preparation.
- Cordes, J. F.; Gunzler, H. *Chem. Ber.* **1959**, *92*, 1055.
- Cox, J. D.; Pilcher, G. *Thermochemistry of Organic and Organometallic Compounds*; Academic Press: New York, 1970.
- Johnson, R. D., III.; Hudgens, J. W. *J. Phys. Chem.* **1996**, *100*, 19874.



- (34) *Computational Thermochemistry: prediction and estimation of molecular thermodynamics*; Irikura, K. K., Frurip, D. J., Eds.; American Chemical Society: Washington, DC, 1998; Vol. 677.
- (35) Tsang, W. Heats of Formation of Organic Free Radicals by Kinetic Methods in Energetics of Organic Free Radicals. In *Energetics of Organic Free Radicals*; Simoes, J. A., Greenberg, A., Liebman, J. F., Eds.; Blackie Academic and Professional: London, 1996; pp 22–58.
- (36) Houle, F. A.; Beauchamp, J. L. *J. Am. Chem. Soc.* **1978**, *100*, 3290.
- (37) Garret, B. C.; Truhlar, D. G. *J. Phys. Chem.* **1979**, *83*, 1052.
- (38) Garret, B. C.; Truhlar, D. G. *J. Phys. Chem.* **1979**, *83*, 1079.
- (39) Truhlar, D. G. *J. Chem. Phys.* **1970**, *53*, 2041.
- (40) Truhlar, D. G.; Isaacson, A. D.; Skodje, R. T.; Garret, B. C. *J. Phys. Chem.* **1982**, 2252.
- (41) Calculations were carried out by a kinetics program developed by C. Gonzalez, National Institute of Standards and Technology, Gaithersburg, MD. The calculations include the symmetrical Eckart's tunneling correction  $G(T)$  described in the following book. Johnston, H. S. *Gas Phase Reaction Rate Theory*; Ronald Press Co.: New York, 1966; pp 38–47.
- (42) Currie, C. L.; Ramsay, D. A. *J. Chem. Phys.* **1966**, *45*, 488.
- (43) Callear, A. B.; Lee, H. K. *Trans. Faraday Soc.* **1968**, *64*, 308.
- (44) Hudgens, J. W.; Dulcey, C. S. *J. Phys. Chem.* **1985**, *89*, 1505.
- (45) Sappey, A. D.; Weisshaar, J. C. *J. Phys. Chem.* **1987**, *91*, 3731.
- (46) Blush, J. A.; Minsek, D. W.; Chen, P. *J. Phys. Chem.* **1992**, *96*, 10150.
- (47) Getty, J. D.; Liu, X.; Kelly, P. B. *J. Phys. Chem.* **1992**, *96*, 10155.
- (48) Nakashima, N.; Yoshihara, K. *Laser Chem.* **1987**, *7*, 177.
- (49) Ha, T. K.; Oth, J. F. M. *J. Phys. Chem.* **1986**, *85*, 1439.
- (50) Chase, M. W., Jr.; Davies, C. A.; Downey, J. R., Jr.; Frurip, D. J.; McDonald, R. A.; Syverud, A. N. *J. Phys. Chem. Ref. Data* **1985**, *14*.
- (51) Wagman, D. D.; Kilpatrick, J. E.; Pitzer, K. S.; Rossini, F. D. *J. Res. Natl. Bur. Stand.* **1945**, *35*, 467.
- (52) Gurvich, L. V.; Veyts, I. V.; Alcock, C. B. *Thermodynamic Properties of Individual Substances*, 4th ed.; Hemisphere Publishing Corp.: New York, 1991; Vol. 2.
- (53) Pedley, J. B. *Thermochemical Data and Structures of Organic Compounds*; Thermodynamics Research Center: College Station, TX, 1994.
- (54) Frenkel, M.; Kabo, G. J.; Marsh, K. N.; Roganov, G. N.; Wilhoit, R. C. *Thermodynamics of Organic Compounds in the Gas State*; Thermodynamics Research Center (TRC): College Station, TX, 1994.